exposes nonideal behavior such as finite op-amp slew and current drive, putting limitations on the *rates* at which an array can be addressed by a real interface. In time these further issues will be analyzed, and the tradeoffs arising there will be better understood.

References

[1] P. Armstrong, "Tactile sensing on the Utah/MIT dextrous hand," Dept. of Comp. Sci., Columbia Univ., New York, NY, Tech. Rep., 1988.

[2] S. C. Jacobsen, I. D. McCammon, K. B. Biggers, and R. P. Phillips, "Design of tactile sensing systems for dextgrous manipulators," *IEEE Control Syst. Mag.*, vol. 8-1, Feb. 1988.

[3] W. D. Hillis, "A high resolution image touch sensor," *Int. J. Robotics Res.*, vol. 1, no. 2, 1982.

[4] B. Tise, "A compact high resolution piezoresistive digital tactile sensor," in *Proc. Conf. Robotics Automat.*, 1988.

[5] H. Van Brussel and H. Belien, "A high resolution tactile sensor for part recognition," in *Proc. 6th Int. Conf. Robot Vision and Sensory Control*, Paris, France, June 1986, pp. 48–58.

Design Concept Development of a Spherical Stepper for Robotic Applications

Kok-Meng Lee and Chi-Kong Kwan

Abstract—**This communication presents the design concept of a new spherical stepper motor capable of three-degrees-of-freedom (DOF) motion in a single joint. The ball-joint-like motor has no singularities except at the boundary of the workspace and can perform isotropic manipulation in all three directions. Due to its relatively simple ball-like structure, undesired cross-coupling and centrifugal components of wrist rotor dynamics can be effectively minimized or eliminated. The spherical stepper motor has potential in robotic applications as a three-DOF shoulder or an eyeball as well as a wrist actuator. In particular, this work presents the systematic conceptualization of a spherical stepper and the feasibility of constructing the spherical stepper. By pointing out the significant differences between a three-DOF spherical motor and the conventional stepper motor, this work illustrates the fundamentals of the spherical stepper design for robotic applications. Along with the experimental data, an analytical approach based on the permeance formula was employed to predict the driving forces generated by a neodymium-iron (Nd-Fe) permanent magnet. The force-displacement curves provide useful information for rational spherical motor design and control.**

I. Introduction

Recent developments in robotics, data-driven manufacturing, and high-precision assembly have provided the motivation for the unusual designs of electromechanical transducers. A flurry of research activities is currently underway in direct drives involving dc, stepping, and brushless electromechanical actuators to improve performance by eliminating the problems inherent in gear systems such as backlash, friction due to meshing, and mechanical compliance. These devices are normally employed to accomplish a single-degree-of-motion manipulation at each joint. In some applications, such as high-speed plasma and laser cutting, the demands on the workspace and the wrist force/torque requirements are low, but the end effector is oriented quickly, continuously, and isotropically in all directions. The performance of the popular three-consecutive-rotational-joints wrist, which possesses singularities within its workspace [1], [2], is less than optimum.

An alternative design based on the concept of a spherical stepper motor presents some attractive possibilities by combining pitch, roll, and yaw motion in a single ball-joint-like actuator. William *et al.* [3], [4] and Laithwaite [5] performed the original analysis on one form of spherical induction motor. Here, the application was in speed control for one-rotational-axis achieved by controlling the direction of the stator wave excitation at an arbitrary angle to the motor axis. Since the work in [3]–[5], little attention has been given to the spherical motor, with the exception of the design of a rotodynamic pump [6] and in gyroscope applications [7], [8]. A spherical induction motor was conceptualized in [9]. The authors presented a detailed analysis of the device based on a field-theoretic concept. This original development was suggested as a robotic wrist actuator in [10]. However, realization of a prototype spherical induction motor remains to be demonstrated. The mechanical design of a spherical induction motor is complex. Laminations are required to prevent movement of unwanted eddy currents. Complicated three-phase windings must be mounted in recessed grooves in addition to the rolling supports for the rotor in a static configuration. These and other considerations led to an investigation of an alternative spherical actuator based on the concept of a variable-reluctance (VR) stepper motor, which is easier to manufacture [11]. The tradeoff, however, is that a sophisticated control scheme is required.

The ball-joint-like characterized with no singularities in the middle of the workspace presents a major performance advantage in trajectory planning and control. Potential applications include actuation for a three-DOF shoulder and an eyeball as well as a wrist. With the shoulder and the wrist joints driven by the spherical motors and the elbow (revolute joint) driven by a single-axis motor to improve reach and dexterity, only three actuators are needed for a total of seven DOF's. As compared to conventional robotic actuation, which would require a total of 14 actuators in a dual-arm manipulator system, the design using three-DOF actuators would significantly improve the kinematic and dynamic characteristics, and thus allow more sophisticated intelligence to be implemented.

In this communication, the design concept of a spherical wrist motor based on the principle of a hybrid permanent magnet and a VR stepper motor is presented. We highlight the fundamental differences between the principle of operation of the three-DOF spherical motor and that of the conventional single-axis stepper motor. A permeance-based model was employed to predict the driving forces generated by a Nd-Fe permanent magnet, the high coercivities of which were first observed in Nd-Fe alloys by Yanus and Drozhzhina [12]. However, permanent magnets containing Nd-Fe have been developed only very recently. It is now generally recognized that these and similar iron-based alloys will be of great importance in a wide variety of applications, particularly in electric motors [13].

II. Ideal Spherical Wrist Actuator

In performing trajectories following tasks, the desired kinematic characteristics of an ideal wrist are no singularities and isotropic manipulation in all three directions. These features are particularly important for applications where high-speed isotropic manipulation of the end-effector is required smoothly and continuously in all directions. In addition, an ideal joint is characterized by the following dynamics: 1) The rotor can be freely suspended so that there are no frictional forces between the rotor and the stator. 2) The spherical hollow rotor is fully balanced such that the moment of inertia $I_{ij} = I\delta_{ij}$ where $\delta_{ij} = 1$ if $i = j$ and $\delta_{ij} = 0$ if $i \neq j$. Thus, the rotor dynamics are completely decoupled and Euler's equation of motion becomes $\tau_i = I\alpha_i$ where α_i and τ_i are the angular acceleration and the resultant torque about the ith body axis. Ideally, the

Manuscript received February 23, 1989; revised January 30, 1990. This work was jointly supported by the School of Mechanical Engineering and the Computer Integrated Manufacturing System Program at the Georgia Institute of Technology.

The authors are with the George W. Woodruff School of Mechanical Engineering, Georgia Institute of Technology, Atlanta, GA 30332.

IEEE Log Number 9041937.

1042-296X/91/0200-0175$01.00 ©1991 IEEE

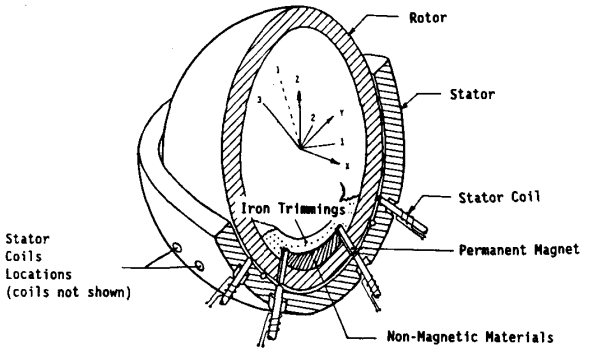

Fig. 1. Conceptual schematic of a spherical wrist motor.

rotor has no moment of inertia, i.e., $I = 0$. The actuating torque is then directly available to overcome the load. 3) The spherical motor consumes no power in static loading conditions. An additional requirement is that a robotic wrist actuator must have a specified torque-to-weight ratio to minimize loading effects on the manipulator arm.

The ball-joint-like wrist actuator has no singularities except at the boundary of the workspace and can perform isotropic manipulation in all three directions. Due to its relatively simple ball-like structure, the undesired cross-coupling and centrifugal components of the wrist rotor dynamics can be effectively minimized or eliminated. With a thin-wall spherical hollow rotor, the spherical stepper motor is essentially a low-inertia robotic wrist. Thus, the ball-joint-like wrist actuator has the kinematic and dynamic characteristics approaching that of an ideal wrist joint.

III. Design Concept

A spherical stepper is conceptualized as shown in Fig. 1. It must be pointed out that the model shown in the figure does not represent an optimum configuration. The model was chosen primarily because of its usefulness in demonstrating concept feasibility. The motor consists of a hemispherical stator that houses the stator coils and a rotor that houses a pair of permanent magnets. The rotor is supported freely by means of air bearings or gimbals.

A. Principle of Operation

The spherical stepper may operate on the principle of a VR motor. The stator coils can be energized individually using the control circuitry. As a pair of the stator coils adjacent to the permanent magnets is energized so that a magnetic field and a corresponding flux are generated, the tangential components of the magnetic forces attract the adjacent magnets and hence exert a resultant torque on the rotor. Appropriate sequencing of high current pulses excites the stator coils, and as a result, the rotor produces a movement in any direction desired.

The principle of operation of the three-DOF spherical stepper differs significantly from that of the single-axis step motor. The primary difference is the required number of energized coils at any particular static orientation for mechanical stability and for three-DOF motion control. As the conventional VR step motor is constrained physically to rotate about one axis, only one force is necessary to actuate or to lock the motion of the rotor in that direction. However, the spherical stepper has an infinite number of rotational axes and has three degrees of freedom. With only one energized coil, the permanent magnet, as a point on the rotor surface, can be actuated in any direction along a tangential inner surface of the stator and thus provide two-DOF motion control on the tangent surface. To provide the third DOF motion control, which is the spin motion about an axis through the center of the rotor and the point of attraction, a second force must be generated by the attraction between an additional active coil and a second permanent magnet to result the spin motion. Hence, for stability of the rotor at a static position or for three-DOF motion, two forces that are not colinear with the center of the rotor are necessary at any instant to provide motion control of the rotor. Unlike the conventional design, which generates three orthogonal components of the external torque, a spherical motor that combines the roll, yaw, and pitch motions in a single joint has the ability to generate the resultant torque in the required direction directly.

The second difference stems from the fact that the maximum number of coils that can be evenly inscribed on a spherical surface is finite. The locations of the evenly spaced coils can be determined by building a polyhedron, which is a three-dimensional solid with polygons as faces (sides). For equal spacing, regular congruent polygons such as equilateral triangles, squares, or pentagons must be used. A point of a polyhedron makes up a convex polyhedral angle. Pythagoras and Plato [14] have shown that a complex polyhedral angle must be made up of at least three faces and must be less than 360° to form a closed polyhedron. Using these principles, it can be shown that the maximum number of coils that can be evenly spaced on a sphere is 20, the figure corresponding to the number of complex angles of a dodecuhedron. However, as the positions of the coils with respect to the stator are generally known for a specified design, the functionality of the spherical stepper does not require that the coils be evenly spaced, although an unevenly or approximately evenly spaced structure would demand more sophisticated control circuitry. To achieve a high positional resolution, an approximately evenly spaced coil arrangement must be developed.

B. Structure of the Spherical Stepper

A particular structure of spherical stepper, as shown in Fig. 2, is proposed to illustrate the feasibility of prototype construction. The fundamental structure consists of a rotor, a stator, a pair of permanent magnets, and the measurement system. The spherical rotor, which houses the permanent magnets and the output shaft, is of nonmagnetic material. As a bearing surface, the rotor surface must be constructed of hard materials and machined to a spherical shape. The stator structure is designed to support the coils, the iron trimmings, the bearings, and the position-measuring devices. The spherical rotor is supported by six bearings. The bearings are adjusted radially and are arranged so that they are evenly spaced 120° apart on two planes located at $Z = r\cos\phi_1$ and $r\cos\phi_2$, where r, ϕ_1, and ϕ_2 are defined in Fig. 2. Similarly, the actual air gap can be adjusted by positioning the coils radially. This design eliminates the necessity to ground the inner surface of the stator to tight tolerance. The following illustrates the fundamentals of the bearing assembly, the coil arrangement, and the measurement system of the spherical stepper.

1) Bearing Assembly: Fig. 2(a) shows an example of a bearing assembly or gimbal. The bearing assembly consists of 1) a fork-like shaft that is supported by a pair of ball bearings and is allowed to rotate freely about its polar axis,, and 2) a roller that is supported at an offset to allow rotation about an orthogonal axis. The spherical rotor is physically in contact with the roller. At the contact point, the reaction force component F_x would result in a rotating motion about the roller axis, and the reaction force F_y would result in a moment that spins about the polar axis of the fork-like shaft. The reaction force component F_z is necessary to maintain physical contact between the roller and the spherical rotor.

To illustrate the fundamental of the rotor support, consider a plane that consists of three gimbals evenly spaced at 120° on the rotor surface of radius r. The translation motion of a rotor body-coordinate-frame can be physically constrained by the inner surface of the stator. However, an excessive external payload may result in slipping at the contact in the direction perpendicular to the plane formed by the gimbals, and this may result in clogging of the rotor motion. Thus, for practical design considerations at least one additional gimbal must be mounted perpendicular to the plane formed by the three gimbals. The gimbals may be mounted on the inner surface of the stator.

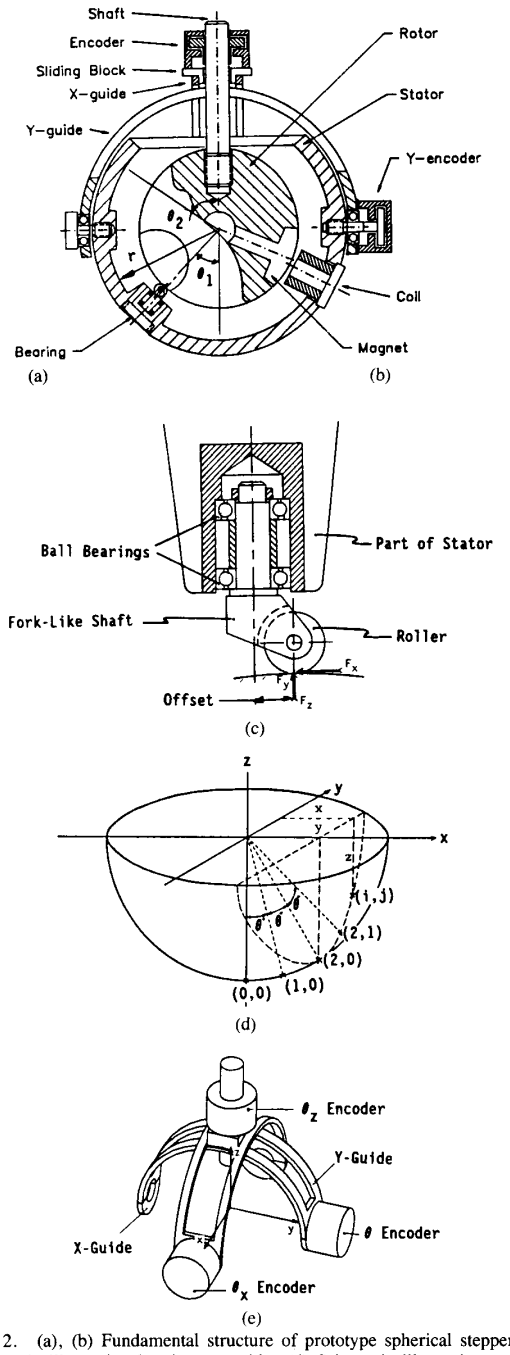

Fig. 2. (a), (b) Fundamental structure of prototype spherical stepper. (c) Schematic illustrating bearing assembly. (d) Schematic illustrating coil arrangement. (e) Schematics illustrating measurement system.

2) Coil Arrangement: To achieve high positional resolution, a scheme was devised to space the coils on the lower hemisphere of the stator as evenly as possible. The position of every coil is represented by the following mathematical relation, as illustrated in Fig. 2(b). The inner surface of the stator is described by the spherical surface ST, the radius by r, and the coil positions by an array of points CP. The spacing between the points is set by the angular parameter θ, which is in degrees and is positive.

TABLE I
COIL SEPARATION TABLE

(Distance is in millimeters.)

(0, 0)*	16.6	(1, 0)	16.6	(2, 0)	16.6	(3, 0)	16.6	(4, 0)	16.6	(5, 0)
16.6		16.6		16.6		16.6		16.6		16.6
(0, 1)	16.6	(1, 1)	16.7	(2, 1)	16.9	(3, 1)	17.6	(4, 1)	20.4	(5, 1)
16.6		16.6		16.6		16.6		16.6		
(0, 2)	16.6	(1, 2)	17.0	(2, 2)	17.9	(3, 2)	20.3	(4, 2)		
16.6		16.6		16.6		16.6				
(0, 3)	16.7	(1, 3)	17.5	(2, 3)	19.5	(3, 3)				
16.6		16.6		16.6		16.6				
(0, 4)	16.7	(1, 4)	18.1	(2, 4)	21.5	(3, 4)				
16.6		16.6		16.6						
(0, 5)	16.8	(1, 5)	18.9	(2, 5)						

*( ) indicates coil index (i, j)

$$ST = \{(X, Y, Z): X^2 + Y^2 + Z^2 = r^2;\ Z \le 0.0 \text{ and } (X, Y, Z) \in R^3,\ r \in R\}$$

$$CP = \{[(X, Y, Z), (i, j)]: (X, Y, Z) \in ST \text{ and } (i, j) \in I\}$$

$$[(X, Y, Z), (i, j)] \in CP$$

iff $X = r \sin(i\theta)$ and if $j = 0$ then

$$y = 0 \text{ and } Z = -r \cos(i\theta)$$

or if $j \neq 0$, there exist $[(a, b, c), (i, j\text{-sgn}(j))] \in CP$ s.t.

$$(X, Y, Z) \cdot (a, b, c) = r^2 \cos\theta.$$

It has been shown that the least number of attractions to provide locking of the rotor is two. For a given pair of magnets, the above arrangement of stator coils determines the primary resolution, which is defined by the spacing of the coils. Further improvement of resolution can be achieved by increasing the number of magnet pairs, modifying the radius of the rotor, or microstepping control between adjacent coils. An example of coil arrangement is displayed in Table I.

3) Measurement System: The measurement of the rotor orientation with respect to the stator can be achieved using the measurement system as shown in Fig. 2(c). The system consists of two circular guides that are made to rotate by the output shaft attached to the rotor. The circular guides are arranged perpendicular to each other such that they can be rotated freely about the x axis and about the y axis of the stator coordinate frame. The angular rotation of the circular guide with respect to the stator frame is measured by means of an encoder. A third encoder measures the angular rotation of the output shaft with respect to one of the outer guide. Thus, the body coordinate frame fixed on the output shaft with respect to the stator can be defined in terms of the encoder readings.

IV. TORQUE PREDICTION

Since the rotor has only three orientation freedoms, any external force acting on the rotor through its center of gravity must be supported by the reaction forces through the air bearings or gimbals. The external moments, however, must be balanced by the restoring torque of the magnetic system, which is determined in terms of the geometry and the current of the exciting coils.

For any given rotor orientation, the tangential force component due to the magnetic attraction between P_j and Q_i can be described as

$$F_j = |F_j| \frac{P_j - TQ_i}{|P_j - TQ_i|} \tag{1}$$

where P_j is the position vector of the jth rotor tooth with respect to the rotor body-coordinate system O-xyz. Q_i is the position vector of the ith stator coil with respect to the stator body-coordinate

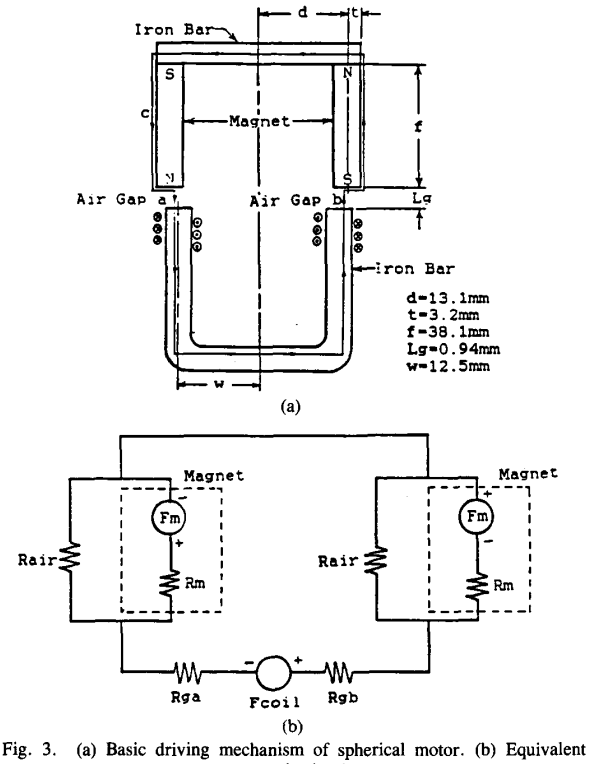

Fig. 3. (a) Basic driving mechanism of spherical motor. (b) Equivalent magnetic circuit.

system O–XYZ. T is the coordinate transformation matrix of stator body-coordinate system O–XYZ with respect to the rotor body-coordinate system O–xyz. The restoring torque due to the electromagnetic attraction between P_j and Q_i is

$$\tau_j = P_j \times F_j. \tag{2}$$

The net restoring torque is the vector sum of all these individual torques generated.

A. Reluctance Force Prediction by Permeance-Based Model

It has been shown that the least number of attractions to provide locking of the rotor is two. Thus, if the surfaces of the coils and the magnets are much smaller than the radius of the spherical rotor surface, the basic driving mechanism of the spherical motor, as represented by the schematic in Fig. 3(a), can be employed as a simplified model to illustrate the reluctance force generating process. Although the analysis was conducted using two poles to illustrate the fundamentals for clarity, the extension to multiple permanent magnet arrangement follows similar guidelines.

The permeance-formula suggested by Chai [15] was employed to predict the reluctance force as a function of displacement. The general assumptions are as follows: 1) The relationship between the magnetomotive force and the magnetic flux is linear. 2) The permeability of the iron parts in the system is assumed to be infinite as compared to that of the air. 3) The assumed flux patterns are given in the Appendix. With these assumptions, the magnetic stored energy can be determined from an equivalent magnetic circuit as shown in Fig. 3(b). The permanent magnet in the circuit is modeled as an mmf source with an internal reluctances R_m and a leakage through the air space R_{air}. The leakage flux of the magnet through the reluctance of the air space R_{air} surrounding the magnet cannot be neglected since the permeability of the magnet is of the same order as that of the air. The air gaps are characterized by the reluctance R_{ga} and R_{gb}.

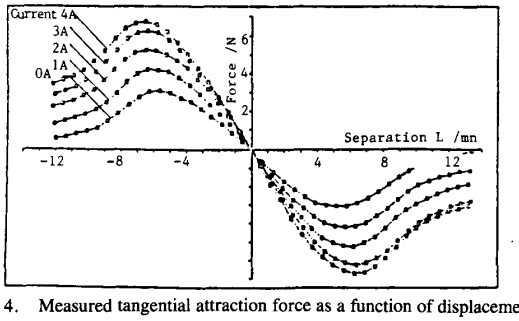

Fig. 4. Measured tangential attraction force as a function of displacement.

From the principle of virtue work, it can be derived that the components of the reluctance force F_i along the ith axis at the air gap are

$$F_i = -\frac{1}{2}\left[\frac{\Gamma}{R_t}\right]^2 \frac{d}{dx_i}\left(R_{ga} + R_{gb}\right) \tag{3}$$

where Γ is the magnetic flux flow through the equivalent magnetic circuit with resultant reluctance R_t derived using Thevenin's theorem. The reluctance of each element can be evaluated from the reciprocal of the permeance [15]. The derivation of the permeance for the particular geometries is summarized in the Appendix.

B. Experimentally Predicted Reluctance Force

It is generally expected that the magnetization curve of the magnets is nonlinear. To aid the design and analysis of the spherical stepper, an experimental prediction of the reluctance forces as a function of the air-gap separation using a pair of neodymium-iron-boron permanent magnets NDFEB-27 was performed on the system,

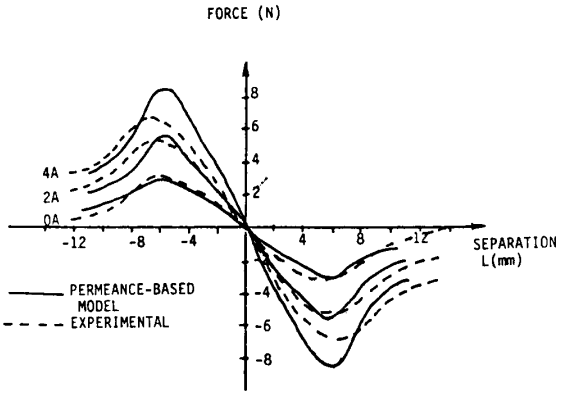

Fig. 5. Comparison between permeance-based model and experimental data.

as shown in Fig. 3(a). Each of the coils has a total of 600 turns on an iron bar of 1/4-in diameter.

The tangential component of the static force was measured by means of strain gages as a function of the coil current and spacing. The results are displayed in Fig. 4. The magnetic system, consisting NdFe-based magnets, has a high tangential force-to-area ratio of 5 N/cm^2 measured with no current excitation, where the area refers to the cross-sectional area of both magnets at the air gap. Each of the magnet weighs 12 g. A maximum force of 3.1 N was obtained even with no current flowing through the coil due to the presence of the permanent magnets. The maximum forces of 4.2, 5.2, 6.2, and 6.7 N were obtained experimentally with a current of 1, 2, 3, and 4 A, respectively. The force was not significantly increased as the current was raised higher than 4-A, thus showing signs of magnetic saturation. The attraction force reached its peak at approximately ± 5.5 mm. At that particular position, the magnet and the U-bar are about 2/7th overlapped. Also, the rate at which the force decreases for separations larger than 5.5 mm does not seem to be affected by the coil current. Given the magnetic property and geometry of the driving magnetic system, the displacement at which the force-displacement curve exhibits a peak can be considered as an optimal stator coil spacing. Further increase of the spacing between stator coils may result in a nonrecoverable condition due to the decay of restoring force with distance.

Comparisons between the analytical predictions and the experimental data are displayed in Fig. 5. The permeance-based model, which predicts the force-displacement curve, is summarized in the Appendix. The permeance-based model and the measured force are in good qualitative agreement. In addition, the model gives a reasonably good prediction of the location of the peak. However, the linearized model overestimates the tangential force for the current higher than 2 A due to the nonlinearities, such as magnetic saturation, as expected.

The use of permanent magnets as rotor magnetic teeth tends to result in a stable static holding torque, but it also indicates that multiple firing when switching from one step to another may be necessary for spherical stepper. In particular, if the relative separation between the coils is large, the attraction force created by the coil current may not be large enough to break the attraction between the magnetic teeth on the rotor and its present matching stator teeth. A reverse current may be necessary to neutralize this "undesired" attraction between the magnets and the stator teeth. Furthermore, the rotor may move toward the adjacent stator teeth instead of the targets because of external disturbances. Hence, to provide stable switching of the spherical motor, the stator teeth adjacent to the targeted teeth are energized in the reverse direction whereas the targeted stator teeth may not have to be excited to attract the rotor teeth.

VI. Conclusion

The design concept of a three-DOF VR spherical stepper for robotic applications was presented. The functionality as well as the feasibility of constructing the fundamental structure of the spherical stepper was demonstrated. The analytical methodology for torque prediction and its limitation were discussed. It is expected that the fundamentals presented in this work provide a basis for future theoretical research in prototype design, dynamic modeling, design optimization, and control scheme development of a three-DOF spherical stepper. In particular, the results were supported with experimental data to provide a rational prediction of maximum static torque generated by the basic driving mechanism, which consists of NdFe-based permanent magnets. Comparisons between the prediction using a permeance-based model and the experimental data show qualitative agreement. The success of the permeance-based model depends significantly on the assumed flux pattern. Currently, research is being conducted in the use of a finite-element package (ANSYS written by Swanson) to provide an understanding of magnetic fields and reluctance force in the spatial coordinate to aid prototype design.

Appendix

Permeance-Based Model

By using Thevinin's theorem, the parallel network (Fig. 3(b)), which consists of the reluctance of the air R_{air} and the mmf and the reluctance of the permanent magnet, F_m and R_m, can be reduced to an equivalent source F_{eq} in series with an equivalent reluctance R_{eq}. The equivalent mmf and reluctance are given as

$$F_{eq} = \frac{R_{air}}{R_{air} + R_m} F_m \tag{A1}$$

$$R_{eq} = \frac{R_{air}}{R_{air} + R_m} R_m. \tag{A2}$$

Thus, the overall magnetic circuit consists of the total mmf which drives the magnetic fluxes Γ through the total reluctance R_t. The total mmf is the sum of the equivalent mmf F_{eq} and the total ampere-turns $(NI)_{coil}$. The total reluctance is the sum of $2R_{eq}$, R_{ga}, and R_{gb}, which can be computed as the reciprocal of the respective permeances.

For the particular electromagnetic system, as shown in Fig. 2 with the equivalent magnetic circuit as given in Fig. 6, the permeance of the magnet is:

$$P_m = \frac{\mu 2}{f}(2t) \tag{A3}$$

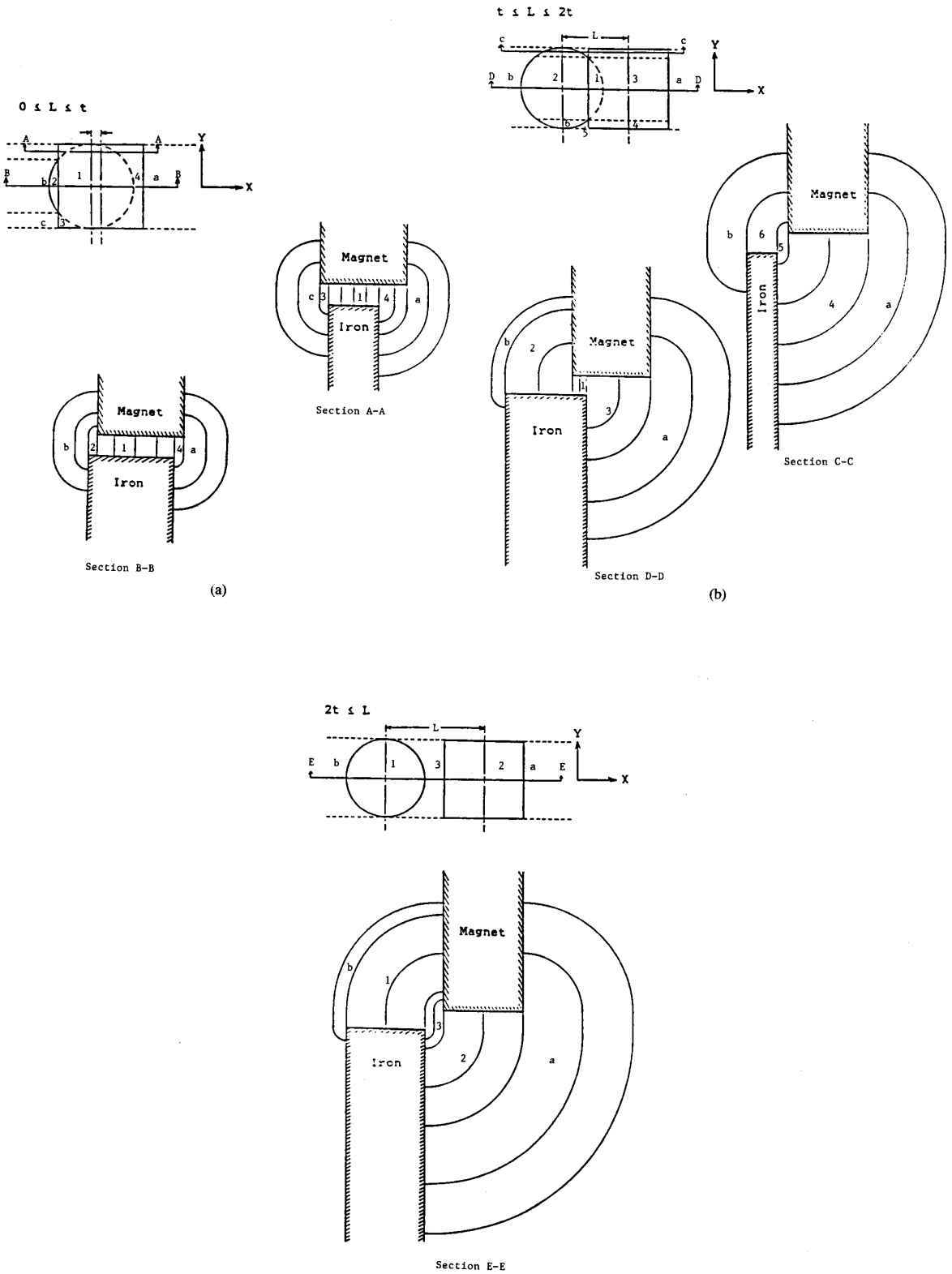

Fig. 6. (a) Assumed flux line pattern in the air gap. Case A: $0 \leq L \leq t$. (b) Case B: $t \leq L \leq 2t$. (c) Case C: $2t \leq L$.

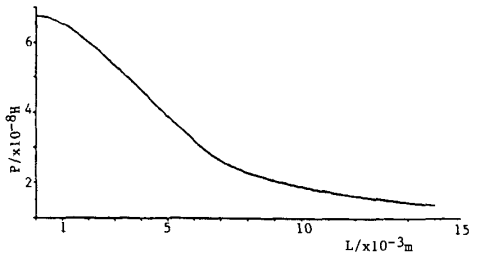

Fig. 7. Permeance of the air gap versus separation.

where μ is the permeability of the magnet ($\mu = 5 \times 10^{-6}$ H/m). Since the magnetic fluxes do not cross each other, the flux in the air space surrounding a magnet would occupy, at the most, half of the air space between the two magnets. The permeance of the air space surrounding the magnet is, therefore, approximated as

$$P_{\text{air}} = \frac{\mu_0}{f}\left[\pi d^2 - (2t)^2\right]. \tag{A4}$$

The arc-straight line method, as suggested by Chai [15], was used to model the air-gap permeance. The assumed flux patterns are shown in Fig. 6 and the corresponding permeance was numerically integrated. The computed permeance of the air gap as a function of separation is shown in Fig. 7.

The equivalent mmf was obtained semi-empirically with the aid of (4). The loop integration is evaluated along the path c indicated in Fig. 3(a). The magnetic field strength of the iron is neglected as the permeability of the iron is assumed to be infinite. The equivalent mmf is equal to the sum of $H_g L_g$ and $H_a f$ where H_g and H_a are the magnetic field strength of the air gap and along the path parallel to the magnet, respectively. Since the flux leaving the magnet is perpendicular to the surface of the magnet, it was estimated that the field strength H_a along the surface of the magnet is inversely proportional to the square of the aspect ratio σ, which is defined as the length-to-width ratio of the magnet. Hence,

$$F_{\text{eq}} = \frac{B_r}{\mu_0}\left[L_g + \frac{f}{\sigma^2}\right] \tag{A5}$$

where B_r is the residue induction of the magnet.

Acknowledgment

Stimulating discussions with Dr. K. Devey, Associate Professor in the School of Electrical Engineering at Georgia Tech, are gratefully acknowledged.

References

[1] H. Asada and J. A. Cro-Granlto, "Kinematic and static characterization of wrist joints and their optimal design," in *Proc. IEEE Int. Conf. Robotics Automat.*, 1985.

[2] R. P. Paul and C. N. Stevenson, "Kinematics of robot wrist," *Int. J. Robotics Res.*, vol. 2, no. 1, pp. 31-38, 1983.

[3] F. William, E. Laithwaite, and L. Piggot, "Brushless variable-speed induction motors," *Proc. IEEE*, pp. 102-118, June 1956.

[4] F. Williams, E. Laithwaite, and G. F. Eastham, "Development of design of spherical induction motors," *Proc. IEEE*, pp. 471-484, Dec. 1959.

[5] E. Laithwaite, "Design of spherical motors," *Electrical Times*, vol. 9, pp. 921-925, June 1960.

[6] I. Laing and N. Laing, U.S. Patent 4 352 646, "Rotodynamic pump with spherical motor," Oct. 5, 1982.

[7] A. Lebedev and P. Shinyev, "Moments acting in a spherical rotor in a magnetic suspension," *Priborostroegie*, vol. 16, no. 5, pp. 85-88, 1973.

[8] I. Vyssh Uchebn Zaved, "Electromagnetic processes in an asynchronous motor with a spherical hollow rotor," *Electromekh*, no. 11, pp. 1231-1239, Nov. 1976.

[9] K. Davey and G. Vachtsevanos, "The analysis of fields and torques in a spherical induction motor," *IEEE Trans. Magn.*, vol. MAG-23, Mar. 1987.

[10] G. J. Vachtsevanos, K. Davey and K-M. Lee, "Development of a novel intelligent robotic manipulator," *Control Syst. Mag.*, June 1987.

[11] K-M. Lee, G. Vachtsevanos, and C-K. Kwan, "Development of a spherical wrist stepper motor," in *Proc. Int. IEEE Conf. Robotics Automat.*, Philadelphia, PA, Apr. 24-29, 1988.

[12] R. Yanus and V. Drozhzhina, "A new magnetic alloy with a very large coercive force," *Nature*, vol. 135, pp. 36-37, Jan. 1935.

[13] G. A. Jubb and R. A. McCurrie, "Hysteresis and magnetic viscosity in a Nd-Fe-B permanent magnet," *IEEE Trans. Magn.*, vol. MAG-23, no. 2, Mar. 1987.

[14] D. E. Smith, *Essentials of Plane and Solid Geometry*. Wentworth-Smith Mathematical Series, 1923.

[15] H. D. Chai, "Permeance model and reluctance force between toothed structures," in *Theory and Applications of Step Motor*, B. C. Kuo, Ed. St. Paul, MN: West, 1973.

An Automatic Navigation System for Vision Guided Vehicles Using a Double Heuristic and a Finite State Machine

Koon-Yu Fok and Mansar R. Kabuka

Abstract—**A navigation system for automatic vision guided vehicles has been presented. The system uses an efficient double heuristic search algorithm for path planning. It is capable of avoiding unknown obstacles and recovering from unidentifiable locations. A linked list representation of the path network database makes the implementation feasible in any high-level language and renders it suitable for real-time application. Extensive simulated experiments have been conducted to verify the validity of the proposed algorithms.**

I. Introduction

Robot mobility is necessary in modern industrial environments for a number of functions, such as transportation of workpieces or performance of specific tasks at different stations. Initial efforts in obtaining methods for robot navigation included the use of buried wires [1] and painted lines [2], [3]. The buried wire method is still the most popular among Japanese manufactures of mobile robots [4]. These methods, however, require extensive customization of the working environment and create a large overhead if the robot routes must be changed.

On the other hand, research has concentrated lately on navigation with little or no *a priori* knowledge of the surrounding environment. In particular, navigation in an outdoor environment has received considerable attention. The main issues here include:

1) recognition of the road or path to be followed, and
2) avoidance of any obstacles that might be encountered along the path.

Since there is little *a priori* knowledge, the problem of navigation in these systems is largely dependent on the capabilities of the sensing mechanisms. Most of the current research has concentrated on using visual sensors [5]-[14] sometimes combined with other

Manuscript received September 1, 1987. This work was presented in part at the Florida Artificial Intelligence Research Symposium (FLAIRS), Orlando, FL, May 1988.

The authors are with the Department of Electrical and Computer Engineering, University of Miami, Coral Gables, FL 33124.

IEEE Log Number 9039465.